 DOI: 10.1002/masy.200751219

# Morphology Development in Polymer Fibers undergoing Solvent/Non-solvent Exchange

*Pratyush Dayal, Thein Kyu**

**Summary:** The solvent/non-solvent interchange across the fiber surface affects the morphology of the fiber in various ways. In this paper, simulations have been performed to elucidate the diverse morphologies obtained during spinning of polymer fibers under the presence of a non-solvent. The proposed model deals with a ternary system derived from Cahn-Hilliard equation, alternatively known as Time Dependent Ginzburg Landau-TDGL model B equation, involving the spatio-temporal evolution of concentration order parameter. Depending on the coexistence region of the ternary phase diagram, various fiber morphologies including concentric bands, internal microfibrillar structures, and porous structures were discerned. It may be inferred that the formation of the aforementioned diverse morphologies is a direct consequence of the initial conditions of the starting mixtures in a manner governed by the relative rates of solvent/non-solvent exchange and the dynamics of phase separation.

**Keywords:** morphology; non linear thermodynamics; phase separation; ternary systems

## Introduction

Solution spinning has been a preferred methodology for the production of many types of advanced fibrous materials[1–4] such as gas separation membranes, high strength high modulus fibers, and more recently, electrospun fibers.[5–9] There are two modes of solution spinning being practiced: dry spinning and wet spinning. The dry spinning technique was first employed in an effort to produce rayon fibers, while the wet spinning was first developed to produce acetate fibers from cellulose triacetate. In the wet spinning process the polymer is dissolved in a solvent and is extruded through a spinneret which makes the fiber to elongate. The polymer molecules get stretched and oriented in the extrusion direction. The mutual diffusion of the solvent and the non-solvent molecules takes place across the fiber skin to-and-fro the surrounding fluid. Due to the complex nature of the wet spinning process, the need to understand is imminent and the ultimate control of the process remains a technological challenge.

Recently, the electrospinning has gained renewed interest because of its capability of producing micro-/nano- fibers of various shape and surface topologies. Electrospinning of polymer solutions has been carried out using various polymer concentrations by applying a high voltage across the spinneret and the target. Many novel features of the electrospun fibers have been reported in literature that include fibers with irregular surfaces, collapsed nanotubes, ribbons, beads, among others. Thus, when examining the cross-sections of electrospun fibers, the expected features include uniform circular shapes with or without skin layers, hollow or collapsed tubes as seen experimentally. Rabolt and coworkers[10] reported an interesting development of porous fiber morphology, who electrospun the polymer solution into humid environment. The extent of porosity depends on many factors one of which is the humidity in the surrounding air. The complex mechanism of pore formation may be attributed to vapor induced phase separation caused by humid environment in which the fiber is spun. During the course of the spinning

Department of Polymer Engineering, the University of Akron, Akron, Ohio-44325
E-mail: tyku@uakron.edu

process the water vapors from the air diffuse into the polymer solution as the solvent escapes, causing the solution to phase separate into polymer lean and polymer rich regions. As the fiber dried out, the low polymer concentration regions appear as voids on the surface. Although obtaining porous materials via phase separation has been known in the past,[11,12] elucidation of this concept to electrospun polymer fibers is indispensable.

In the present manuscript, a theoretical simulation has been conducted to elucidate the effect of solvent/non-solvent exchange across the fiber interface boundary on the morphology development in polymer fibers formed by the electrospinning process. The modeling involves non-equilibrium thermodynamics via the nonlinear reaction-diffusion equation, i.e., a combination of Cahn-Hilliard time-evolution equation[13,14] for non-solvent transfer into the phase separating fiber core and the Fick's law[15] for the solvent escape to the surrounding non-solvent environment. The proposed nonlinear reaction-diffusion equation is capable of describing the spatio-temporal development of fiber morphology.

## Model Description

Let us consider a polymer fiber with a circular cross-section which initially contains a binary solution of polymer and solvent. When spinning is carried out into the non-solvent environment, there is a net outward flux of solvent and a net inward flux of non-solvent across the fiber boundary. Now the system within the fiber becomes a ternary solution containing polymer, solvent, and non-solvent. As the non-solvent gets into the fiber, the system becomes unstable, with respect to concentration, due to the decline in the solvent quality, thereby resulting in phase separation. The process of liquid-liquid phase separation of such a ternary fluid mixture may be modeled by modifying the Flory-Huggins- Staverman [16] (FHS) theory of mixing (Gibbs function) to a ternary case, i.e.,

$$f = \frac{\phi_1}{n}\ln\phi_1 + \phi_2\ln\phi_2 + \phi_3\ln\phi_3 + \chi_{12}\phi_1\phi_2 + \chi_{13}\phi_1\phi_3 + \chi_{23}\phi_2\phi_3 \qquad (1)$$

where, $n$ is number of statistical segments of the polymer, $\chi_{12}$, $\chi_{13}$, $\chi_{23}$ are the FHS interaction parameters between polymer and solvent, polymer and non-solvent and solvent and non-solvent, respectively while $\phi_1$, $\phi_2$, $\phi_3$ are the volume fractions of polymer, solvent and non-solvent, respectively.

In the present case, we simplify the system such that the solvent acts like an athermal solvent to the polymer in question (i.e. $\chi_{12} = 0$) and also there is virtually no interaction between solvent and non-solvent or at least de-mixing does not take place (i.e. $\chi_{23} = 0$). In practice, these aforementioned interactions between polymer/solvent and solvent/non-solvent and polymer/non-solvents must be considered to generate diverse morphologies; however, these simplistic assumptions may be adequate for the present purpose. Setting $\chi_{13} = 3.0$ and $n = 10$, a hypothetical phase diagram is solved self-consistently by balancing the chemical potentials of each component in each phase in conjunction with a double tangent algorithm.

## Governing Equations

This modified FHS free energy density is then incorporated into the Cahn-Hilliard[13,14] (CH) time-evolution equation, alternatively known as Time Dependent Ginzburg-Landau (TDGL) - model B equation[17] by incorporating the non-local interface gradient terms of de Gennes, viz.,[18,19,21]

$$F = \int_V \left( \frac{\phi_1}{n}\ln\phi_1 + \phi_2\ln\phi_2 + \phi_3\ln\phi_3 + \chi_{12}\phi_1\phi_2 + \chi_{13}\phi_1\phi_3 + \chi_{23}\phi_2\phi_3 + \frac{1}{36}\sum_{k=1}^{3}\frac{a_k^2}{\phi_k}(\nabla\phi_k)^2 \right) dV \qquad (2)$$

 

where, $a_k$ is the statistical segment lengths of the component $k$ and bold 'nabla' symbol signifies vector operation.

According to the Cahn-Hilliard theory, the rate of change of concentration or polymer volume fraction, $\phi_i$ in time for a binary system may be expressed in terms of the gradient of the chemical potentials in vector form (bold symbol), is given by,

$$\frac{\partial \phi_i}{\partial t} = \nabla \cdot \Lambda \nabla \frac{\delta F}{\delta \phi_i} \tag{3}$$

in which the functional derivative is given as $\delta/\delta\phi_i \equiv \partial/\partial\phi_i - \nabla \cdot \partial/\partial\nabla\phi_i$. This description may be extended to a ternary system under consideration by following the standard definition of the chemical potential[18] as,

$$\mu_k = F + \sum_{j=1}^{m} \frac{\delta F}{\delta \phi_j}(\delta_{kj} - \phi_j) \tag{4}$$

where $\mu_k$ is the chemical potential of component $k$, $\delta_{kj}$ is the Kronecker delta. Thus, one obtains the expressions for chemical potential differences among each phase from Equation (4) as,

$$\begin{aligned}\mu_2 - \mu_1 = (1 + \ln\phi_2) - \frac{1 + \ln\phi_1}{n} \\ + \chi_{12}(\phi_1 - \phi_2) - \chi_{13}\phi_3 + \chi_{23}\phi_3 \\ + \frac{1}{36}\left(\frac{a_1^2}{\phi_1^2}(\nabla\phi_1)^2 - \frac{a_2^2}{\phi_2^2}(\nabla\phi_2)^2\right) \\ + \frac{1}{18}\left(\frac{a_1^2}{\phi_1}\nabla^2\phi_1 - \frac{a_2^2}{\phi_2}\nabla^2\phi_2\right)\end{aligned} \tag{5}$$

$$\begin{aligned}\mu_3 - \mu_1 = (1 + \ln\phi_3) - \frac{1 + \ln\phi_1}{n} - \chi_{12}\phi_2 \\ - \chi_{13}(\phi_1 - \phi_3) + \chi_{23}\phi_2 \\ + \frac{1}{36}\left(\frac{a_1^2}{\phi_1^2}(\nabla\phi_1)^2 - \frac{a_3^2}{\phi_3^2}(\nabla\phi_3)^2\right) \\ + \frac{1}{18}\left(\frac{a_1^2}{\phi_1}\nabla^2\phi_1 - \frac{a_3^2}{\phi_3}\nabla^2\phi_3\right)\end{aligned} \tag{6}$$

The equation of continuity can be expressed in terms of the chemical potential differences[18] between the individual phases in what follows,

$$\frac{\partial \phi_2}{\partial t} = \nabla \cdot [\Lambda_{22}\nabla(\mu_2 - \mu_1) - \Lambda_{23}\nabla(\mu_3 - \mu_1)] \tag{7}$$

$$\frac{\partial \phi_3}{\partial t} = \nabla \cdot [-\Lambda_{23}\nabla(\mu_2 - \mu_1) + \Lambda_{33}\nabla(\mu_3 - \mu_1)] \tag{8}$$

where,

$$\begin{aligned}\Lambda_{23} &= \frac{\Lambda_{0,22}\Lambda_{0,33}}{\Lambda_{0,11} + \Lambda_{0,22} + \Lambda_{0,33}}; \\ \Lambda_{22} &= \frac{\Lambda_{0,22}(\Lambda_{0,11} + \Lambda_{0,33})}{\Lambda_{0,11} + \Lambda_{0,22} + \Lambda_{0,33}}; \\ \Lambda_{33} &= \frac{\Lambda_{0,33}(\Lambda_{0,11} + \Lambda_{0,22})}{\Lambda_{0,11} + \Lambda_{0,22} + \Lambda_{0,33}}\end{aligned} \tag{9}$$

The Onsager kinetic coefficient, $\Lambda_{0,kk}$, of component $k$ is given by,[19,20]

$$\Lambda_{0,kk}(q) = 6D_k n_k \phi_{k,0} \frac{1 - \exp(-n_k a_k^2 q^2/6)}{n_k a_k^2 q^2} \tag{10}$$

where $D_k$ is the self-diffusion coefficient of component $k$ and $q$ is the wavenumber. Equation (7) and (8) afford the evolution of volume fractions of solvent and non-solvent. The volume fraction of the polymer at a given time can be computed using the conserved relation, viz., $\phi_1 = 1 - \phi_2 - \phi_3$.

As a first approximation one can assume that there is no phase separation at the boundary hence the gradient of the chemical potential can be approximated to gradient of the concentration. This approach is valid so long as the phase separating system reverts to a single phase. In our previous papers,[22,23] we have demonstrated that the Fick's diffusion equation,[15] is a special case of the Cahn-Hilliard time evolution equations in which the system is treated in the context of a single well-potential while setting the interface gradient term of the concentration field to be zero. Thus in the absence of external flow the flux, $\mathbf{J}_k$ for solvent/non-solvent interchange may be expressed as,

$$\mathbf{J}_2 = -\alpha_{2,0}\nabla\phi_2 \tag{11}$$

$$\mathbf{J}_3 = \alpha_{3,0}\nabla\phi_3 \tag{12}$$

 

where $\alpha_{k,0}$is diffusivity of component $k$. Equation (11) and (12) have opposite signs that signify the flows in the opposite directions. Since solvent escapes through the outer surface of the fiber to the non-solvent bath or the surrounding medium (or air) saturated with non-solvent, but the volume fraction of solvent in surrounding medium is negligibly small, and thus it is taken as zero outside the boundary of the outer skin. Concurrently, the non-solvent diffuses into the fiber through the interface.

## Simulation Scheme

Since the CH time-evolution or TDGL-model B equations, derived from equation of continuity, are only valid for conserved systems, it is necessary to modify the boundary conditions by adopting a quasi steady state assumption (QSSA) to abide by the mass conservation law in the model-B equations. Equation (7) and (8) were solved numerically using a finite difference method employing a second-order central difference scheme in space and a first-order forward difference in time using Equation (11) and (12) as boundary conditions. Initially the system has a circular cross-section with a particular radius and the boundaries are updated at every time step. The simulation was performed in Eulerian space in dimensionless units using a cylindrical grid of $256 \times 128 \times 32$. The initial distribution of polymer in the system was considered homogeneous, but the concentration fluctuation was introduced by thermal noise that obeys the fluctuation-dissipation theorem.

## Results and Discussion

Figure 1 depicts a theoretical phase diagram of a ternary system consisting of polymer, solvent, and non-solvent where the dark thick line represents the binodal curve and the thin line signifies the spinodal line. The gap between the spinodal and the

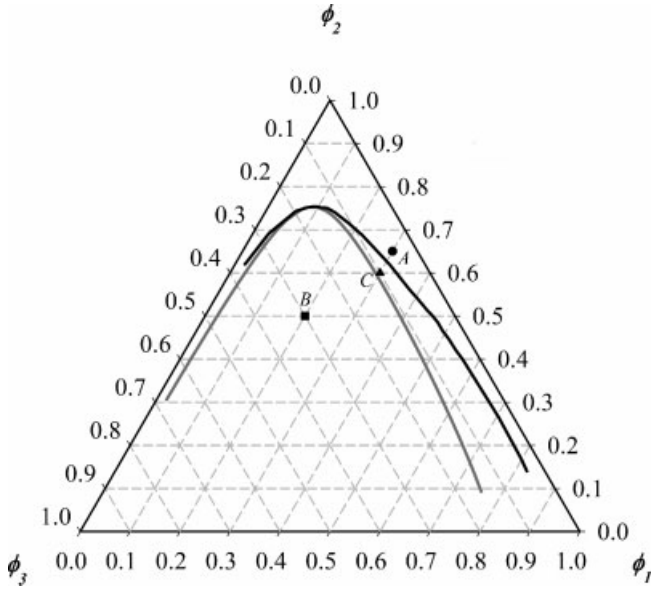


***Figure 1.***
Ternary phase diagram of a polymer (1), solvent (2) and non-solvent (3) system. The interaction parameters $\chi_{12} = \chi_{23} = 0$ and $\chi_{13} = 3.0$. The solid gray line represents the spinodal curve while the solid black line represents the binodal curves. Points *A*, *B* and *C* represent the initial concentration of the polymer/solvent/non-solvent mixture.

 

binodal curves is known as the metastable region whereas the envelope under the spinodal curve represents the unstable region. The actual phase diagram of a ternary system would be a three-dimensional surface, but only the slice of such a phase diagram at a given temperature is shown in Figure 1. It should be noted that more complicated ternary phase diagrams do exist in the literature (for e.g. see ref [24]);

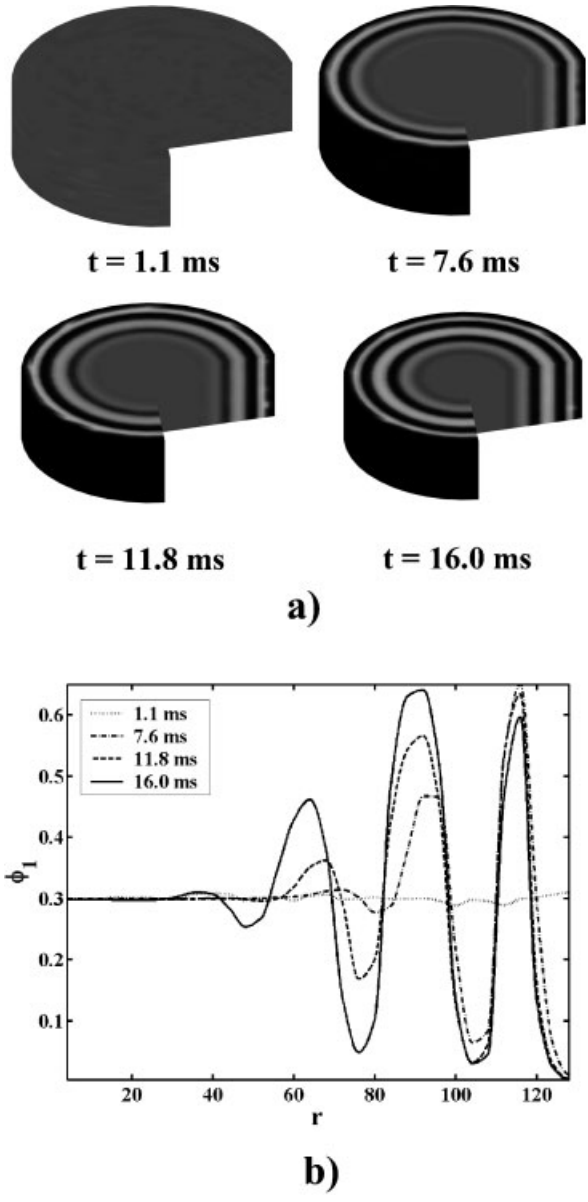


***Figure 2.***
Formation of concentration bands for a system represented by point *A* in the phase diagram. (a) Time sequence shows not only the single phase structure in the core of the fiber but also shrinkage in volume of the fiber as a result of solvent loss from its surface. (b) Cross-sectional profile of the polymer concentration shows oscillations at the surface which decrease in amplitude towards the core. The parameters utilized were: $\phi_1 = 0.30$, $\phi_2 = 0.65$, $\phi_3 = 0.05$, $\alpha_{2,0}/\Lambda_{23} = -1.0$, and $\alpha_{3,0}/\Lambda_{23} = 0.0$.

 

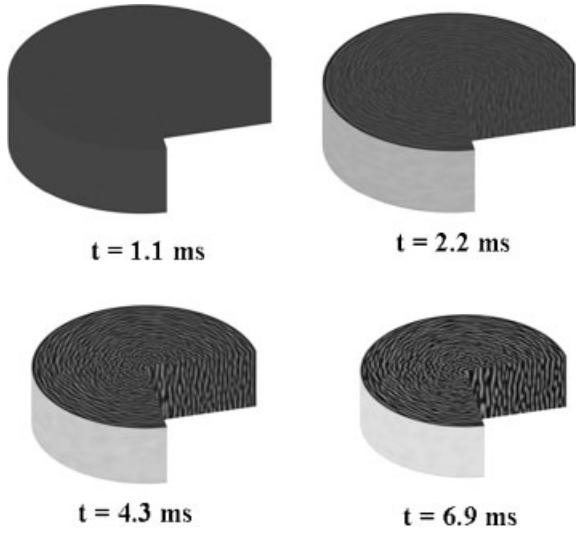


***Figure 3.***
Spatio-temporal evolution of polymer concentration showing a smooth fiber surface with bi-continuous core. The starting concentrations, denoted by point *B* in the phase diagram, ensure that the system is in the unstable two-phase region, initially. The surface concentration is driven into the single phase region of the phase diagram by virtue of solvent loss, resulting in a smooth fiber surface while the interconnected structure persists in the core as a result of spinodal decomposition. The parameters utilized were: $\phi_1 = 0.20$, $\phi_2 = 0.50$, $\phi_3 = 0.30$, $\alpha_{2,0}/\Lambda_{23} = -0.1$, and $\alpha_{3,0}/\Lambda_{23} = 0.001$. The change in the volume of the fiber is also noticeable.

however, we shall consider the simplest form as described below.

The volume fractions of the starting mixture are represented by points *A*, *B* and *C*. To mimic the spatio-temporal evolution of phase separated domains, we carried out the numerical simulation of the CH equations for the ternary polymer/solvent/non-solvent system using the following parameters[25]: $\Lambda_{0,11} = 10^{-10}\mathrm{m}^2/\mathrm{s}$ for polymer, $\Lambda_{0,22} = 10^{-9}\mathrm{m}^2/\mathrm{s}$ for solvent, and $\Lambda_{0,33} = 10^{-9}\mathrm{m}^2/\mathrm{s}$ for non-solvent. Moreover, the correlation distances of polymer, solvent, and non-solvent were considered to be the same for simplicity with the value of $a_k = 10^{-7}\mathrm{m}$. It is adequate to simultaneously solve Equation (7) and (8), because only two of the three parameters are independent, i.e., $\phi_1 + \phi_2 + \phi_3 = 1$.

Figure 2 exhibits the time sequence for the formation of concentration bands represented by the cross-sectional profile of the polymer volume fraction. The initial conditions, viz., $\phi_1 = 0.30$, $\phi_2 = 0.65$, $\phi_3 = 0.05$ with $\alpha_{2,0}/\Lambda_{23} = -1.0$ and $\alpha_{3,0}/\Lambda_{23} = 0.0$, correspond to point *A* in Figure 1. Initially the system is in the one-phase stable region. With the progression of time, the average concentration of the non-solvent increases that pushes the system into the unstable two-phase region. The outward flux of the solvent generates a solitary kink wave in the concentration field and the concentration at the boundary moves into the unstable region. The wave front thus generated propagates towards the center of the fiber via diffusion. In the unstable region, the system attempts to stabilize by approaching towards the equilibrium (binodal lines) compositions. However, when the instability exceeds a certain threshold value, the front wave transforms into an oscillatory wave, thereby revealing multiple concentration bands (Figure 2b). The wavelength (or periodicity) and velocity of such waves may be estimated according to the selection rules through the dispersion relationship as described elsewhere.[27,28] The diameter of the fiber also gets shrunk due to the net solvent loss

 

resulting from the difference in the rates of solvent/non-solvent exchange. It should be pointed out that the formation of such banded texture is well documented in polymer liquid crystals[26,27] and biological systems.[29]

We shall now examine the system corresponding to the initial volume fractions at point $B$ ($\phi_1 = 0.20$, $\phi_2 = 0.50$, $\phi_3 = 0.30$) as depicted in Figure 1 having different solvent ($\alpha_{2,0}/\Lambda_{23} = -0.01$) and non-solvent ($\alpha_{3,0}/\Lambda_{23} = 0.001$) diffusivities.

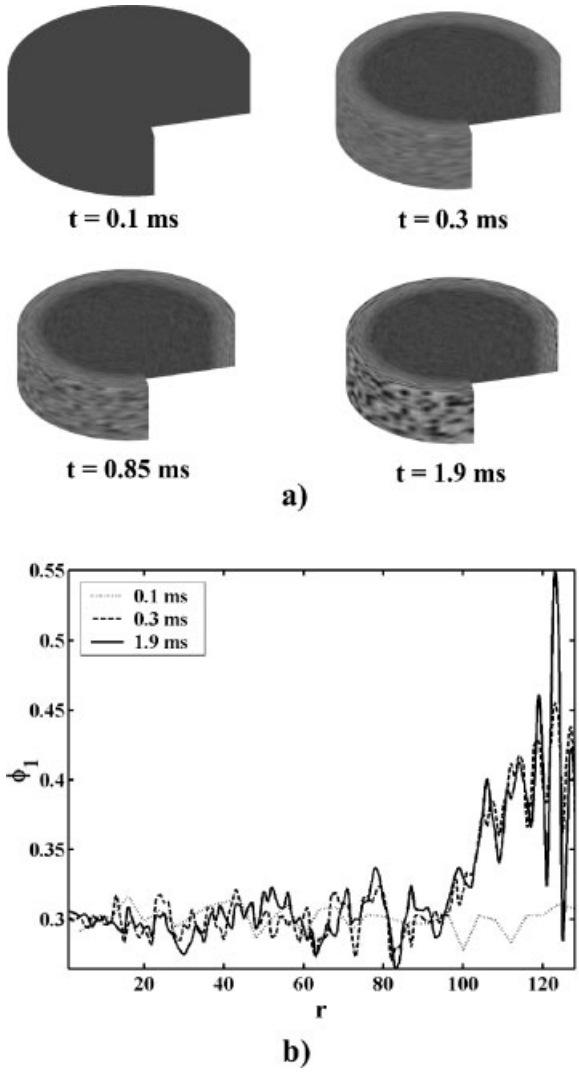


***Figure 4.***
Formation of porous fiber as a result of phase separation at the fiber surface. The starting concentrations correspond to point C of the phase diagram. (a) Time sequence reveals the volume shrinkage as well as porous surface morphology, resulting from phase separation, as the system is pushed into the unstable two-phase region. (b) Cross-sectional profile of polymer concentration shows amplification of the thermal noise at the surface. The parameters utilized were: $\phi_1 = 0.30$, $\phi_2 = 0.60$, $\phi_3 = 0.01$, $\alpha_{2,0}/\Lambda_{23} = -0.01$, and $\alpha_{3,0}/\Lambda_{23} = 0.001$.

 

Figure 3 shows the spatio-temporal evolution of the fiber structure, exhibiting the smooth fiber surface with the microfibrillar structure in the core. Since, the outward-flow of the solvent is an order of magnitude larger than the inward-flow of the non-solvent, and hence, the concentration of the polymer at the surface is pushed into the stable one-phase region thus suppressing the phase separation at the fiber surface. Moreover, the solvent/non-solvent exchange across the fiber surface does not significantly affect the fiber core structure showing a bi-continuous structure which in turn suggests, although by no means a proof, the occurrence of phase separation through the SD mechanism. This bi-continuous morphology is akin to the microfibrillar texture obtained by Dayal et al.[23] for a binary system.

In order to obtain porous fiber, it is necessary to change the initial conditions of the simulation and also the relative rates of solvent/non-solvent exchange to ensure the polymer concentration at the surface does not exit to the single phase region during the time period of simulation. Point *C* in Figure 1 corresponds to such a condition in which the parameters utilized were: $\phi_1 = 0.20$, $\phi_2 = 0.60$, $\phi_3 = 0.10$, $\alpha_{2,0}/\Lambda_{23} = -0.1$ and $\alpha_{3,0}/\Lambda_{23} = 0.001$. Figure 4a illustrates the snapshots of evolved morphology in which the reduction in the fiber diameter is due to the net loss of the solvent. It can be noticed that the system is in the metastable region initially. With the time progression, the interface of polymer/non-solvent propagates into the unstable two phase region. At a later time, the formation of pores on the fiber surface can be discerned clearly (Figure 4a). As evident in Figure 4b, the core of the fiber also gets rougher as the phase separating front advances inward. The thickness of the skin depends on the relative rates of solvent/non-solvent exchange. Unlike the previous case of the undulated structures in Figure 2, the concentration profiles at the outer surface are irregular due to the porous nature of the fiber surface which is more pronounced relative to the core. These findings are in good agreement with the findings of Casper and coworkers[10] that explains the ingress of the non-solvent from the surface of the fiber causing the liquid-liquid phase separation thereby resulting in porous appearance.

*Acknowledgements:* The support of the National Science Foundation, (Grant Numbers DMR 0209272 and DMR 0514942) and the Ohio Board of Regents through the Research Challenge Grant for the present work is gratefully acknowledged.

[1] R. J. E. Cumberbirch, J. E. Ford, R. E. Gee, *Shirley Inst. Mem.* **1961**, *34*, 9.
[2] J. Corbriere, "*Man-Made Fibers Science and Technology*", Vol. *1* , O. Sczbolcs, I. Szabolcs, Eds., Interscience, New York **1967**.
[3] G. J. Capone, "*Acrylic Fiber Technology and Applications*", Mercel Dekker Inc., New York **1995**.
[4] A. Ziabicki, "*Fundamentals of Fiber Formation*", J. Wiley & Sons, New York **1976**.
[5] J. S. Kirn, D. H. Reneker, *Polym. Eng. Sci.* **1999**, *39*, 849.
[6] H. Fong, I. Chun, D. H. Reneker, *Polymer* **1999**, *40*, 4585.
[7] D. H. Reneker, I. Chun, *Nanotechnology* **1996**, *7*, 216.
[8] S. Koombhongse, W. Liu, D. H. Reneker, *J. Polym. Sci. Part B: Polym. Phys.* **2001**, *39*, 2598.
[9] A. L. Yarin, S. Koombhongse, D. H. Reneker, *J. Appl. Phys.* **2001**, *89*, 3018.
[10] C. L. Casper, J. S. Stephens, N. G. Tassi, D. B. Chase, J. F. Rabolt, *Macromolecules* **2004**, *37*, 573.
[11] P. van de White, P. J. Dijkstra, J. W. A. van den Berg, J. Feijen, *J. Membr. Sci.* **1996**, *117*, 1.
[12] C. Chandavasu, M. Xanthos, K. K. Sirkar, C. G. Gogos, *J. Membr. Sci.* **2003**, *211*, 167.
[13] J. W. Cahn, I. E. Hilliard, *J. Chem. Phys.* **1958**, *28*, 258.
[14] J. W. Cahn, *Acta Metall.* **1961**, *9*, 795.
[15] R. B. Bird, W. E. Stewart, E. N. Lightfoot, "*Transport Phenomena*", Wiley, New York **1994**.
[16] P. J. Flory, "*Principles of Polymer Chemistry*", Cornell University Press, Ithaca **1953**.
[17] J. D. Gunton, M. S. Miguel, P. S. Sahni, "*Phase Transitions and Critical Phenomena*", C. Domb, J. L. Lebowitz, Eds., Academic Press, New York **1983**.
[18] M. Takenaka, T. Hashimoto, *Macromolecules* **1996**, *29*, 4134.

 

[19] K. Kawasaki, K. Sekimoto, *Physica* **1987**, *143A*, 349.
[20] P. Pincus, *J. Chem. Phys.* **1981**, *75*, **1996**.
[21] P. G. de Gennes, *J. Chem. Phys.* **1980**, *72*, 4756.
[22] A. J. Guenthner, S. Khombhongse, W. Liu, P. Dayal, T. Kyu, *Macromol Theory Simul* **2006**, *15*, 87.
[23] P. Dayal, T. Kyu, *J. Appl. Phys.* **2006**, *100*, 043512.
[24] S. Blonski, W. Brostow, D. A. Jonah, M. Hess, *Macromolecules* **1993**, *26*, 84.
[25] "*Perry's chemical engineers' handbook*", 7th edition, R. H. Perry, D. W. Green, Eds., McGraw-Hill, New York **1997**.
[26] T. Kyu, P. Zhuang, P. Mukherjee, *Am. Chem. Soc. Symp. Ser.* **1989**, *384*, 266.
[27] A. J. Guenthner, T. Kyu, *Macromolecules* **2000**, *33*, 4463.
[28] G. Dee, J. S. Langer, *Phys. Rev. Lett* **1983**, *50*, 383.
[29] M. Bezzi, A. Ciliberto, A. Mengoni, *J Bio Phys* **1999**, *25*, 279–288.

 